

Structural, Vibrational and Mechanical Studies of Hydroxyapatite produced by wet-chemical methods

K. Donadel, M. C. M. Laranjeira*, V. L. Gonçalves,
V. T. Fávere,

Depto de Química, Universidade Federal de Santa Catarina, Florianópolis, Santa Catarina, Brazil, Cx. P. 476, 88040-900

K. D. Machado, J. C. de Lima,

Depto de Física, Universidade Federal de Santa Catarina, Florianópolis, Santa Catarina, Brazil, Cx. P. 476, 88040-900

L. H. M. Prates

Depto de Estomatologia, Universidade Federal de Santa Catarina, Florianópolis, Santa Catarina, Brazil, Cx. P. 476, 88040-900

Abstract

Hydroxyapatite samples were produced by two different wet-chemical methods, and characterized by x-ray diffraction, infrared and compression strength measurements. The x-ray diffraction measurements were simulated using the Rietveld method, and structural data as lattice parameters and average crystallite size were obtained. The infrared spectra showed the presence of CO_3^{2-} ions in all samples, indicating a contamination by these ions. By mixing samples produced by both methods, a bioceramic was obtained and, after sintering, samples with very high compression strengths (26–30 MPa) were obtained.

Key words: Hydroxyapatite, x-ray diffraction, mechanical properties.

PACS: 61.10.Nz, 81.05.Cy, 81.07.Bc, 81.20.Ev

* Corresponding author.

Email addresses: mauro@qmc.ufsc.br (M. C. M. Laranjeira),
kleber@fisica.ufsc.br (K. D. Machado).

1 Introduction

Calcium hydroxyapatite, $\text{Ca}_{10}(\text{PO}_4)_6(\text{OH})_2$ (CaHAp), is the main inorganic component of hard tissues of the bones of vertebrates. It answers for 60–70% of the mineral phase in the human bone [1,2,3], and it is a member of the ‘apatite’ family of compounds. Biological apatites, which comprise the mineral phases of tissues like enamel, dentin and bone, usually have compositions and crystallinity slightly different from the stoichiometric CaHAp. These structural differences are responsible for different physical and mechanical properties found for these materials. In the body, they were usually observed to be carbonate (CO_3^{2-}) substituted and calcium deficient [4]. Bone tissue has the ability to regenerate, forming healthy tissue that grows in the direction of the damaged tissue in order to repair it. So, if a material with physical and chemical properties similar to the biological bone constituents could be produced, the growth process of healthy tissue can be accelerated and the recovery time of the patients can be decreased, for instance. Such materials should also have porosity and compression strength similar to the tissues they will substitute, in order to assure biocompatibility. Successful experiments on animals (rats, rabbits and dogs) led to clinical application of CaHAp bioceramics in humans over the last two decades. These experiments included the grafting of periodontal defects, post-traumatic long bone defects and augmentation of the alveolar ridge and maxillofacial skeleton [5,6,7,8,9,10].

To produce synthetic CaHAp with the desired properties, chemical and hydrothermal methods can be used [1,11,12]. In general, these methods allow the production of materials with good crystallinity, physiological stability and with the morphological characteristics of the hard tissues, but some of the physical, chemical and mechanical properties of the final products usually depend on the specific method used in the synthesis. In addition, contaminant phases, such as calcium oxide (CaO) and tricalcium phosphate (α - and β -TCP) can also be formed during the fabrication of CaHAp. Here, we have used a combination of two different methods to produce CaHAp bioceramics, which were studied by x-ray diffraction (XRD) and infrared (IR) spectroscopy techniques. In addition their compression strengths were also measured. The results obtained indicated that the mechanical properties depend on the content of CO_3^{2-} ions incorporated into the CaHAp lattice, which substitute PO_4^{3-} ions, and possibly on the content of Ca^{2+} ions substituted by Mg^{2+} and occasionally Na^+ ions.

2 Experimental Procedures

2.1 Preparation of the samples

2.1.1 Method A

In the method A the samples (hereafter called A-HAp) were prepared in the following way: 0.090 mol of $(\text{NH}_4)_2\text{HPO}_4$ (Nuclear) and 0.152 mol of $\text{Ca}(\text{NO}_3)_2 \cdot 4\text{H}_2\text{O}$ (Nuclear) were completely dissolved in distilled water. Thus, a NH_4OH 25vol% solution is added to the previous solution. The obtained solution is then heated at 65°C for 90 min under stirring. After that, the beaker is sealed, and the solution is heated to its boiling point for 2 h. Then, it is cooled to room temperature and the precipitates were allowed to settle overnight. Next, they were filtered, washed with distilled water in order to keep a pH 7 and dried at 60°C for 4 h. Some amounts of the A-HAp samples were sintered at 900°C in an electrically heated box furnace Jung model 0912 for 1 h and they will be called A-HAp-S [13].

2.1.2 Method B

The samples prepared using method B (hereafter called B-HAp) were produced in the following way: first, a solution (hereafter solution B1) was formed by dissolving 0.182 mol of $\text{Ca}(\text{NO}_3)_2 \cdot 4\text{H}_2\text{O}$ (Nuclear) and 0.0105 mol of $\text{MgCl}_2 \cdot 6\text{H}_2\text{O}$ (Reagen) in 500 ml of distilled water. Then, a second solution (solution B2) was prepared by dissolving 0.387 mol of $\text{Na}_2\text{HPO}_4 \cdot 7\text{H}_2\text{O}$ (Nuclear), 1.25 mol of NaOH (Nuclear), 0.357 mol of NaHCO_3 (Vetec) and 0.00752 mol of $\text{Na}_4\text{P}_2\text{O}_7 \cdot 10\text{H}_2\text{O}$ (Resimap) in 1300 ml of distilled water. Next, the solutions B1 and B2 were put together in a beaker at room temperature and a white precipitate is obtained, which is washed until a pH 8 is reached. Then, the cream was dried at 80°C for 48 h, and a part of it was also sintered at 900°C for 1 h, forming the B-HAp-S samples [14].

2.1.3 Bioceramic Samples

The bioceramic samples (BIO) were prepared by mixing 1 g of A-HAp, 2 g of B-HAp and 1.8 ml of $\text{Na}_2\text{HPO}_4 \cdot 7\text{H}_2\text{O}$ 0.2 M, which acts as an accelerator for the reaction. After that, cylindrical samples of 10 mm height and 5 mm diameter were prepared with the obtained cream, and they were heat treated at 50°C for 2 h. The bioceramic cylinders were also sintered at 900°C for 1 h (BIO-S). In order to perform compression strength comparisons, cylindrical samples of A-HAp and B-HAp were made in the same way, and some of them were also sintered at 900°C .

2.2 X-ray Measurements

X-ray measurements were collected using a Rigaku power diffractometer, Mini-flex model, working with Cu $K\alpha$ radiation ($\lambda = 1.5418 \text{ \AA}$). XRD measurements were taken for all samples produced. The patterns obtained are shown in Sec. 3.

2.3 Infrared Measurements

Infrared measurements were performed from 400 to 4000 cm^{-1} using a FTIR Perkin-Elmer infrared spectrometer. Spectra were taken for A-HAp, B-HAp, BIO and BIO-S samples.

2.4 Compression strength measurements

The compression strength measurements were performed in all samples using a 3M Instron 4444 equipment.

3 Results and Discussion

Figure 1 shows the x-ray pattern for A-HAp and its simulation using the Rietveld refinement procedure [15]. It was indexed to the hexagonal structure of hydroxyapatite given in JCPDS card 730294. As it can be seen from this figure, a good agreement was achieved. The refined lattice parameters obtained were $a = 9.4207 \text{ \AA}$ and $c = 6.8898 \text{ \AA}$. From the refinement and using the Scherrer formula [16], an average crystallite size of 164 \AA was obtained, indicating that it is in the nanometric form. No signals of contamination by β -TCP (tricalcium phosphate) or CaO (calcium oxide) were found in this measurement. After the sintering process, its crystallinity increases, as it can be seen in figure 2, which shows the x-ray pattern for the A-HAp-S sample with its Rietveld refined simulation. Again, there is no contamination by β -TCP or CaO. The new lattice parameters were $a = 9.4236 \text{ \AA}$ and $c = 6.8847 \text{ \AA}$. These lattice parameters are different from those given in the JCPDS card 730294 for hydroxyapatite ($a = 9.432 \text{ \AA}$ and $c = 6.881 \text{ \AA}$). These differences (decrease in a parameter and increase in c parameter) are usually associated with a contamination of the CaHAp lattice by CO_3^{2-} ions [1]. This contamination could be confirmed by the IR measurement performed on the A-HAp sample, shown in fig. 3.a. In this figure, the characteristic bands of hydroxyapatite associated

with PO_4^{3-} ions [17] can be seen around 470, 567, 603, 1035 and 1100 cm^{-1} , and small shoulders can be seen at 967 cm^{-1} , also associated with PO_4^{3-} ions, and at 630 and 3575 cm^{-1} , which are assigned to OH^- ions [2,17]. The broad bands around 1639 and 3447 cm^{-1} are associated with water in the sample [1]. The contamination by CO_3^{2-} ions gives rises to the bands at 870, 1420 and 1465 cm^{-1} , and the small bands around 2030 cm^{-1} are associated with CO_2 vibrational modes, which was probably absorbed from the air [1,12]. The presence of CO_3^{2-} ions can be attributed to some contamination of the starting reagents and also to the air. Two points should be noted here: first, as biological apatite usually have CO_3^{2-} ions, the contamination observed above is not undesirable. Second, in the sintered sample much of water and CO_3^{2-} ions are expelled from the sample. The average crystallite size of A-HAp-S increases to 536 \AA , making it interesting for several biological applications.

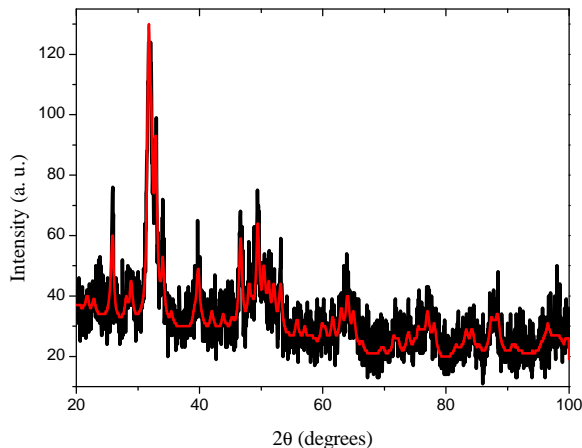


Fig. 1. XRD pattern for A-HAp and its Rietveld simulation.

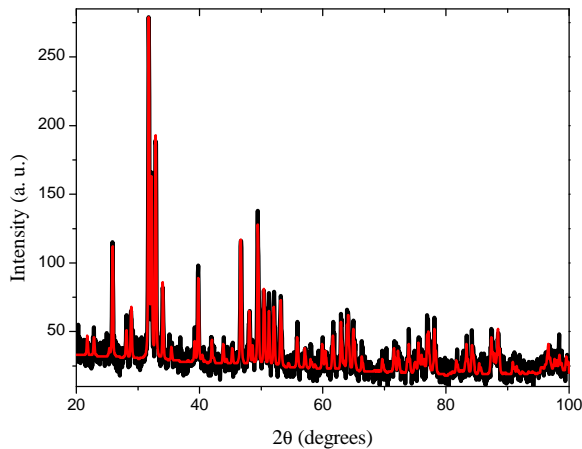


Fig. 2. XRD pattern for A-HAp-S and its Rietveld simulation.

Figure 4 shows the x-ray pattern for B-HAp. It is very similar to that shown in fig. 1, and it was also indexed to the hydroxyapatite phase given in JCPDS card 730294. As it happens for A-HAp, no signals of contamination by β -TCP or CaO were found. Its simulation obtained from the Rietveld refinement is

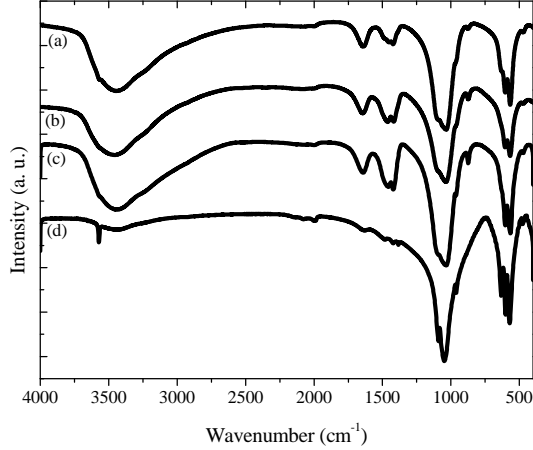


Fig. 3. IR spectra for (a) A-HAp; (b) B-HAp; (c) BIO and (d) BIO-S samples.

also seen in fig. 4, and the refined lattice parameters are $a = 9.4023 \text{ \AA}$ and $c = 6.8877 \text{ \AA}$. There is a large reduction of the lattice parameter a , whereas c increases, in agreement with the fact that now the samples were prepared using reagents containing CO_3^{2-} ions, which causes a larger substitution of PO_4^{3-} for CO_3^{2-} ions. This substitution produces better-defined bands associated with CO_3^{2-} ions, which can be seen in fig. 3.b around 875, 1418 and 1464 cm^{-1} . This figure also shows the bands seen in fig. 3.a for A-HAp. The PO_4^{3-} and OH^- bands are found in the same positions, but the water bands change to 1645 and 3454 cm^{-1} , respectively. Again, there is a small contamination by CO_2 from air. The average crystallite size of this phase is 322 \AA , almost twice of the HAp samples, suggesting that the method used in B-HAp preparation is able to produce samples more suitable for biological applications than the method used in A-HAp.

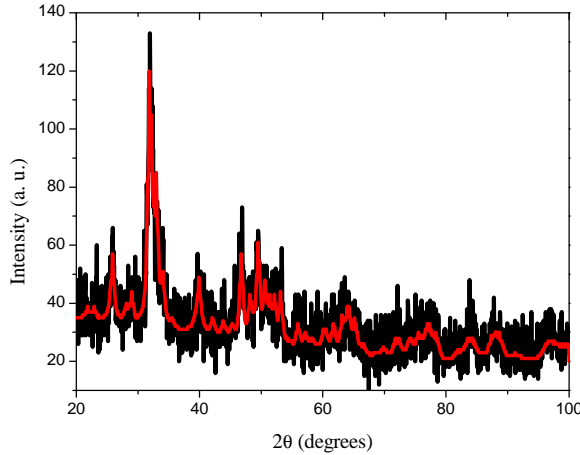


Fig. 4. XRD pattern for B-HAp and its Rietveld simulation.

Figure 5 shows the x-ray pattern obtained for B-HAp-S and its simulation obtained using the Rietveld refinement procedure. It is similar to the pattern shown in fig. 2, and it was also indexed to the hydroxyapatite phase. The

refined lattice parameters obtained were $a = 9.4213 \text{ \AA}$ and $c = 6.8731 \text{ \AA}$, showing an increase in the lattice parameter a and an unexpected large decrease in c , which could indicate a larger release of CO_3^{2-} ions by this sample. In addition, it is known that Mg^{2+} ions can replace Ca^{2+} ions in the hydroxyapatite lattice. Since Mg^{2+} ions are present in the reagents used in method B, this fact could be also responsible for these changes in the lattice parameters. The average crystallite size of B-HAp-S is 467 \AA , a little smaller than that found for A-HAp-S.

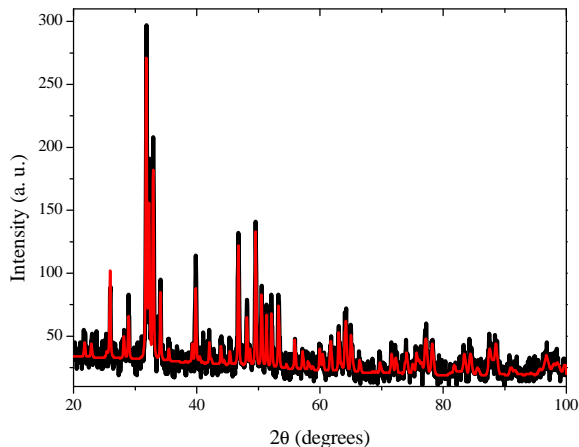


Fig. 5. XRD pattern for B-HAp-S and its Rietveld simulation.

Figure 6 shows the x-ray pattern measured for the BIO-S samples. It is similar to those seen in figs. 2 and 5, and corresponds to the hydroxyapatite phase found in all x-ray patterns above. Its Rietveld simulation is also shown in fig. 6, and the refined lattice parameters are $a = 9.4241 \text{ \AA}$ and $c = 6.8825 \text{ \AA}$. The average crystallite size of BIO-S reaches 561 \AA , showing that this is the sample with the highest degree of crystallinity. The IR spectra measured for these samples before and after the sintering process can be seen in fig. 3.c and 3.d. Fig. 3.c shows the characteristic bands of hydroxyapatite (the PO_4^{3-} vibrations at $470, 567, 603, 1036$ and 1095 cm^{-1}), well defined CO_3^{2-} bands around $873, 1420$ and 1460 cm^{-1} , a OH^- band as a shoulder of the very broad band associated to water at 3448 cm^{-1} , besides the water band at 1644 cm^{-1} and the CO_2 band at 2000 cm^{-1} . After the sintering, the water bands are much reduced, and OH^- bands around 633 and 3568 cm^{-1} are much better resolved. The CO_3^{2-} bands about 1420 cm^{-1} almost disappeared, indicating a great release of CO_3^{2-} ions by the sample.

Although the x-ray measurements of the samples have indicated that the hydroxyapatite phase is present in all samples, some differences among them exist, as can be seen by comparing the lattice parameters and average crystallite sizes obtained, and also the IR spectra seen in fig. 3. However, the most impressive difference is verified in the compression strength measurements performed on the samples. The cylindrical A-HAp samples have compression strengths ranging from 2 to 5 MPa. After sintering, these samples (A-HAp-S)

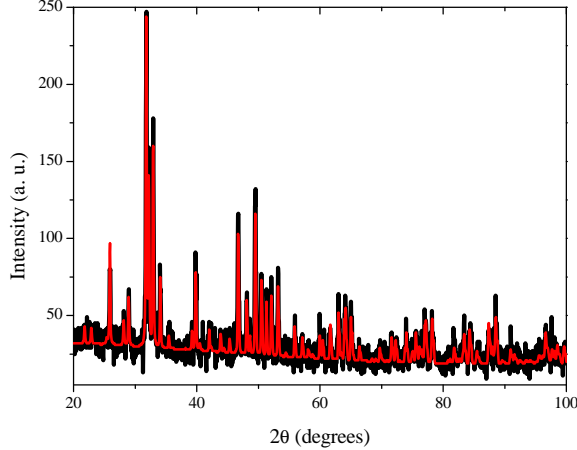


Fig. 6. XRD pattern for BIO-S and its Rietveld simulation.

reach compression strengths of 6-9 MPa. The compression strengths of the cylindrical B-HAp samples are less than 1 MPa, and do not seem to change after sintering (B-HAp-S). Considering now the cylindrical bioceramic samples, their compression strengths changes from 1-2 MPa before sintering (BIO) to 26–30 MPa after sintering (BIO-S), an increase by almost five times when compared to the values found for A-HAp-S and by six times when compared to usual hydroxyapatite values reported in the literature [11,13].

A possible explanation for this fact is that by mixing the samples produced by the two different methods, the contamination by CO_3^{2-} , Mg^{2+} and maybe Na^+ ions decreased and reached an optimal value, which is lesser than that seen in the B-HAp and greater than that found in the A-HAp samples alone. Another possibility is that, although B-HAp and B-HAp-S have those contaminants, their porosity is too large even after sintering, thus decreasing their compression strength. The increase in the compression strength of BIO-S makes it a very good material for biological application in dental and bone implants, for instance. A deeper investigation about the causes of this behavior is in progress and will be published elsewhere.

4 Conclusion

From this study we can conclude that

- (1) Calcium hydroxyapatite, $\text{Ca}_{10}(\text{PO}_4)_6(\text{OH})_2$, was produced by using both methods described in Sec. 2.1, as confirmed by the Rietveld refinements performed on the x-ray diffraction patterns of all samples. The infrared spectra agree with this verification and show the characteristic bands of hydroxyapatite. The crystallinity of all samples improves after the sintering process, as indicated by the increase in the average crystallite

sizes.

- (2) A-HAp samples have a small contamination formed by CO_3^{2-} ions, which is not undesired since biological apatite usually shows about 4% of these ions in its composition. B-HAp samples, besides a higher contamination by CO_3^{2-} ions, also have Mg^{2+} and maybe Na^+ ions in their composition. The contamination by CO_3^{2-} is also confirmed by the infrared spectra of the samples, which show the CO_3^{2-} bands.
- (3) The B-HAp and B-HAp-S samples have a larger porosity than A-HAp and A-HAp-S samples, as confirmed by the compression strength measurements, which indicate that B-HAp and B-HAp-S are too soft materials. Although the compression strength of A-HAp-S increases after the sintering, this value is still low for some dental and bone implant applications.
- (4) The best samples were obtained by mixing the samples produced by the two methods and submitting them to the sintering process, obtaining the BIO-S samples. Their compression strengths reach 26–30 MPa, very suitable for dental and bone implant applications. A possible explanation for the improvement obtained is that, by mixing the samples produced by the two methods, the contamination by CO_3^{2-} and Mg^{2+} ions reached optimal values, increasing the mechanical properties of the samples.

Acknowledgements

We thank to the Brazilian agencies CNPq and CAPES for financial support.

References

- [1] G. Felício-Fernandes, M. C. M. Laranjeira, Calcium phosphate biomaterials from marine algae hydrothermal synthesis and characterisation, *Química Nova* 23 (2000) 441.
- [2] D. Bayraktar, A. C. Tas, Chemical preparation of carbonated calcium hydroxyapatite powders at 37°C in urea-containing synthetic body fluids, *J. Euro. Ceram. Soc.* 19 (1999) 2573.
- [3] M. R. Finisie, A. Josué, V. T. Fávere, M. C. M. Laranjeira, Synthesis of calcium-phosphate and chitosan bioceramics for bone regeneration, *An. Acad. Bras. Cienc.* 73 (2001) 525.
- [4] L. L. Hench, J. Wilson, *An Introduction to Bioceramics*, World Scientific, London, 1993.
- [5] B. V. Rejda, J. G. J. Peelen, K. de Groot, Tricalcium phosphate as a bone substitute, *J. Bioeng.* 1 (1977) 93.

- [6] M. Jarcho, Calcium phosphate ceramics as hard tissue prosthetics, *Clin. Orthop. Relat. Res.* 157 (1981) 259.
- [7] H. M. Rosen, Porous, block HA as an interpositional bone graft substitute in orthognatic surgery, *Plast. Reconstr. Surg.* 83 (1989) 985.
- [8] N. Passuti, G. Daculsi, J. M. Rogez, S. Martin, J. V. Bainvel, Macroporous calcium phosphate ceramic performance in human spine fusion, *Clin. Orthop. Relat. Res.* 248 (1989) 169.
- [9] H. S. Byrd, P. C. Hobar, K. Shewmake, Augmentation of the craniofacial skeleton with porous HA granules, *Plast. Reconstr. Surg.* 91 (1993) 15.
- [10] K. Satoh, K. Nakatsuka, Simplified procedure for aesthetic improvement of facial contour by maxillary augmentation using a porous HA graft for maxillofacial deformity, *Plast. Reconstr. Surg.* 97 (1996) 338.
- [11] D. Tadic, F. Peters, M. Epple, Continuous synthesis of amorphous carbonated apatites, *Biomaterials* 23 (2002) 2553.
- [12] J. G. Morales, J. T. Burgués, T. Boix, J. Fraile, R. R. Clemente, Precipitation of stoichiometric hydroxyapatite by a continuous method, *Cryst. Res. Technol.* 36 (2001) 15.
- [13] N. O. Engin, A. C. Tas, Preparation of porous $\text{Ca}_{10}(\text{PO}_4)_6(\text{OH})_2$ and $\beta\text{-Ca}_3(\text{PO}_4)_2$ bioceramics, *J. Am. Ceram. Soc.* 83 (2000) 1581.
- [14] D. D. Lee, C. Rey, M. Ailova US Pat. 6,214,368 (2001).
- [15] R. A. Young, A. Sakthivel, T. S. Moss, C. O. Paiva-Santos, DBWS-9411 - an upgrade of the DBWS*. * programs for Rietveld refinement with PC and mainframe computers, *J. Appl. Cryst.* 28 (1995) 366.
- [16] H. P. Klug, L. E. Alexander, X-Ray Diffraction Procedures for Polycrystalline and Amorphous Materials, 2nd Edition, John Wiley and Sons, New York, 1974.
- [17] N. Pleshka, A. Boskey, R. Mendelsohn, Novel infrared spectroscopy method on the determination of crystallinity of hydroxyapatite minerals, *Biophys. J.* 60 (1991) 786.